The analytical development pursued by the author is presented in Chapters 4 and 5. With regard to the stationary stability analysis presented in Chapter 4, good experimental correlation was achieved with respect to the laboratory measurements. The definition of the regions of instability of the steady state motion was based on the assumption of a datum solution. The motivation for the datum solution came from a desire to identify regions where the trivial uncoupled lateral *linear* motion was unstable, thus emphasising the importance of the non-linear coupling between the lateral and longitudinal motion and consequently the state of tuning of the system. By applying a harmonic balance method, this approach would directly account for all conditions of tuning obviating the need to consider anomalous or special cases. In light of the experimental results extracted from the laboratory experiment, it would be advantageous to further interrogate the quasi-static equations of motion developed in chapter 5, via a study based on the method of multiple scales. Such a study is currently being pursued at this University (Aligianis[1993]). This study is intended to examine the nonlinear steady state response, and the stability of this response directly for specific tuning conditions of the laboratory model. Further fundamental development is required to examine the system response in the presence of a non-stationary excitation. The simulation of the laboratory model to a swept sine excitation exhibits peculiar behaviour. Such behaviour requires experimental corroboration, as well as fundamental analytical studies in order to assess the implications of such response on the system behaviour with regard to increased winding velocities. This would represent a further extension to the stationary analysis suggested above.

The numerical simulation presented in Chapter 5, illustrated the danger of applying a normal mode technique directly to the equations of motion. This was particularly frustrating, but a worthwhile experience for the author. The initial results from the normal mode simulation were convincing; to the extent that the severity of the problem only became apparent once the laboratory data was available. It is clear from this experience that drawing conclusions based purely on a numerical simulation is a dangerous exercise and should be viewed with skepticism until experimental correlation is achieved. It is in this regard that criticism of the final simulation of the mine hoist system is levelled. The correlation of this system is based on observations provided by Dimitriou and Whillier. Although a video motion analysis system was developed to facilitate such a correlation, and such a study is currently in progress, a number of correlations would be required to convincingly satisfy this criticism. It was decided at this stage to correlate the simulation results broadly with a system which was known by Industry to exhibit adverse dynamic motion, and which had received a great deal of attention in the past, but had not as yet been successfully simulated over the entire ascending and descending winding cycle. Further experimental correlation is clearly necessary, and is currently being

pursued with a major mining house. It is interesting to note that on this particular winder, resonance occurs on the ascending cycle to the extent that the vibration of the headgear superstructure is visible and audible. As a result the winder speed has been reduced from 15 m/s to 13.8 m/s.

The definition of damping mechanisms capable of correctly predicting the lateral and longitudinal dissipation characteristics of mine hoist ropes requires substantial experimental effort. Rudimentary tests were carried out by the author, and a general proportional damping model was applied to model the longitudinal dissipation. Although Mankowski[1988][1990] has examined the lateral dissipation characteristics of a mine hoist rope describing irrotational whirling motion, further studies will be required. The damping mechanism assumed in a dynamic simulation may exert a significant influence on the simulated response, and consequently until accurate data is available, a numerical simulation can be viewed as approximate at best. Conversely, an over ambitious degree of accuracy would be naive.

In the process of developing the analytical model of the mine hoist system, it was assumed that no lateral motion occurs in the vertical rope. Dimitriou and Whillier observed that such motion was related to the adverse catenary motion on the ascending cycle, and hypothesised that it may promote mutual excitation of the catenary via the vertical rope and vice versa. The neglect of the lateral motion in this study was chiefly due to the added complexity associated with accounting for such motion in the discretised model. Such detail would require the incorporation of a substantial number of lateral modes, significantly extending the computational effort. It is the authors' opinion that such detail should be incorporated only after a fundamental appreciation of the system behaviour has been achieved. Simple laboratory tests confirm that violent interactions between the lateral motion on the catenary and vertical section can arise. This represents a further aspect for consideration. Such motion was experimentally monitored on a mine hoist system and is presented in appendix I. A further limitation on the current mine hoist model is that it assumes that the winder is an ideal energy source, and the headgear is rigid. With the advent of advanced winder motors, the electrical winder characteristics are receiving attention in the context of controlling the longitudinal system behaviour due to transients induced during the acceleration and deceleration phase of the winding cycle. This development has been promoted by new legislation which permits the lowering of the rope factor of safety on installations with such control, enabling winding to depths of 4000 m without the use of subshafts. Kaczmarczyk [1993] is currently investigating the simulated response of the hoist system by including the electrical characteristics of the winder motor.

It is natural to question whether an effective strategy exists whereby adverse catenary motion can be corrected or controlled on an existing installation. This is a difficult issue to address, since experience indicates that such strategies ultimately lead to a lowering of the winding velocity, and a consequent loss in production rate. With the advances in control technology and electric motors, it is natural to consider active control strategies. These have not been considered previously. Due to the high drum inertia such strategies cannot be affected directly by the winder. However, it may be possible that if the sheave is energised to equalise the tension between the catenary and vertical system, then an effective strategy may develop to correct such motion. A simulation of the ascending cycle of the Kloof hoist system with a low sheave inertia at 14.8 m/s resulted in a greatly reduced catenary motion. This aspect is currently being investigated with the aid of the laboratory model.

This study has provided a substantial challenge to the candidate. It is natural to be self critical of certain analytical aspects of the work. For instance, it would have been particularly satisfying to complement the simulation of the laboratory model with an analytical study of the steady state motion via the method of multiple scales. The peculiar motion obtained with the non-stationary excitation also represented an attractive avenue of analytical study. In this regard the candidate had to continually redirect the effort towards a practical outcome, even when the analytical aspects of the subject could have been motivated through personal interest. On the otherhand, the experience gained from dealing with a practical system, where it is difficult to obtain physical measurements and quantify the physical parameters accurately, provided valuable experience in that the results achieved required continued critical appraisal.

Clearly further analytical studies are to be pursued in the laboratory and on site to extend this work further. It is hoped that this study will provide support to future researches in the field of mine hoist dynamics, as well as enabling the University to facilitate an informed assessment of existing installations on behalf of the mining industry.

Appendix A

Excitation Definition

This appendix considers the definition of the excitation mechanisms applied in the stationary stability analysis, and in the non-linear numerical simulation of the system. In the stationary stability analysis the excitation accounts for the stationary periodic displacements which occur at the winder drum during constant velocity winding, due to the coiling mechanism. In the numerical simulation, the excitation definition comprises of the former excitation, as well as those excitation mechanisms which give rise to transient system response at various stages of the winding cycle.

During ascent of the conveyance, the winding cycle consists of an initial acceleration to achieve the nominal winding velocity. The conveyance then ascends at a constant winding speed until it decelerates as the conveyance approaches the bank at the head of the shaft. In the process of winding, the rope is coiled onto the drum, and forced displacement excitation occurs at the drum due to the Lebus liner and the resulting coiling pattern. During the constant velocity phase, the excitation imparted to the system via the coiling pattern is periodic and stationary. Since it is not possible to wind the entire length of rope onto the drum in a single layer, multiple layers are required. Typically four layers of rope are wound onto the drum. At the end of a layer, as the rope reaches the drum flange, it changes its traverse direction and rises a full rope diameter to continue coiling on the next layer. The layer change imparts appreciable longitudinal and in-plane lateral transients to the system. Following the layer change, due to the reversal of the traverse direction, the out-of-plane lateral excitation due to the coiling mechanism changes phase by 180° relative to that of the previous layer. Consequently stationary periodic excitation only occurs during the constant velocity phase of the wind, whilst the rope is traversing across the drum surface. Transient excitations occur during the acceleration

and deceleration phases, as well as during a layer change. Thus the excitation applied to the system, and considered in this appendix consists of:

- Longitudinal and lateral in and out of plane stationary periodic excitation due to the Lebus liner coil cross-over profile.
- Longitudinal excitation due to the acceleration/deceleration profile.
- Longitudinal and in-plane lateral excitation due to a layer change.

Other excitation sources not considered in this study may arise due to ovality of the winder drum and head sheave, or due to shaft steelwork misalignment.

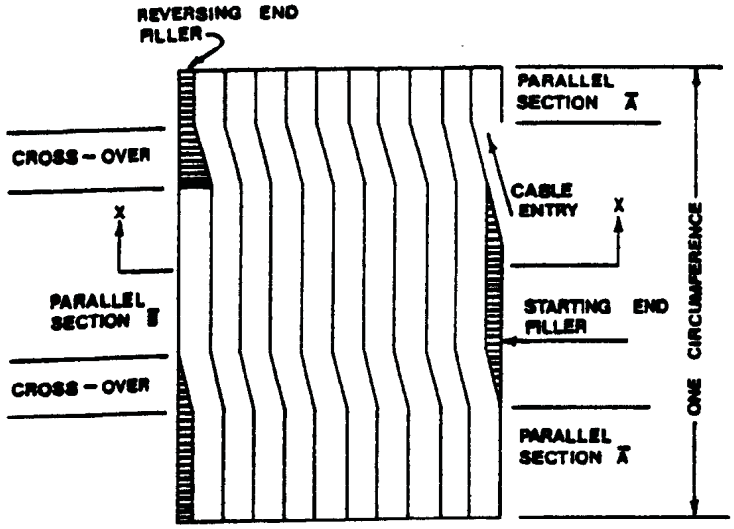

Figure A.1: Mankowski[1982], Figure 2.4(a): Winder drum fitted with a Lebus liner

A.1 Lebus Coil Cross-Over Excitation

Dimitriou and Whillier [1973] identified the Lebus coiling mechanism as the primary source of periodic excitation applied to the system during the constant velocity winding phase. They considered the lateral out-of-plane excitation due to the coiling mechanism to be most significant, and analysed the frequency content of the wave form. In this analysis, they examined a symmetrical 180° Lebus liner, as well as asymmetrical designs with multiple cross over regions. Their analysis demonstrated that in the case of the 180° symmetrical liner, periodic excitation occurred, with a fundamental frequency of twice the angular velocity of the drum. Also the first and second harmonics of the lateral out-of-plane excitation were of a similar order and considered significant. With regard to asymmetrical liners, it was demonstrated that the excitation was periodic with a fundamental excitation at the angular velocity of the drum. The amplitude of the harmonics varied in magnitude with the degree of asymmetry, but no obvious advantage could be found. Since 180° symmetrical Lebus liners are commonly used in the mining industry, the definition of the excitation is based on this configuration.

A 180° lined Lebus drum consists of two parallel grooved circular shells offset from one another by half a rope diameter. The shells are joined at the cross-over insert, which maintains the continuity of the grooves, as illustrated in figure A. Consequently a coil cross-over occurs twice per drum revolution. The cross-over geometry induces excitation in the lateral out of plane w-direction, and in the axial u-direction of the rope. The axial excitation occurs due to the difference in arc length between the diametral arc and that traversed at the cross-over interface. Excitation normal to the drum or in the in-plane v-direction occurs on the second and higher layers as a consequence of the rope rising over underlying coils of the lower layers.

The lateral in-plane displacement of the rope on the second rope layer is calculated from the geometry of the underlying layer as illustrated in figure A.2.

$$v = (1 - \frac{\sqrt{3}}{2})d$$

On the third layer the rope will rise through twice this distance, whilst on the fourth layer it will rise through three times this distance etc. Thus accounting for the layer number, n:

$$v_n = (n-1)(1 - \frac{\sqrt{3}}{2})d$$

where v_n represents the in-plane amplitude during the n^{th} layer.

When the rope exits from the cross-over region, its total displacement is half a rope diameter in the out-of-plane lateral direction, relative to the entry position. Thus the magnitude of the lateral out-of-plane displacement is:

$$w = \frac{d}{2}$$

The magnitude of the displacement in the u direction can be calculated by considering the geometric properties of the cross-over region as illustrated in figures A.3,A.2. During a cross-over the axial velocity of the rope increases to accommodate the difference between the arc length traversed through a cross-over, and that which would be traversed in the absence of a cross-over. Thus relative to the nominal axial displacement due to the winding velocity, this difference represents the additional axial displacement applied to the system. This difference is calculated as:

$$u = R_d\beta[1 + (\frac{d}{2R_d\beta})^2 + (\frac{2v_n}{R_d\beta})^2]^{\frac{1}{2}} - R_d\beta$$

$$u \approx (0.125 + 0.018(n-1)^2)\frac{d^2}{R_d\beta}$$

Figure A.4 illustrates the physical motion of the rope in the u, v, w directions for one rotation of the drum[1]. The motion in the u direction illustrates that the average winding velocity is slightly larger than that of the peripheral velocity of the drum. This is reflected by the dotted line in figure A.4 (a). The periodic component of the longitudinal motion is consequently the motion relative to this line, as presented in figure A.5 (a). The lateral in-plane displacement v due to the rope rising over an underlying coil is presented in figure A.4 (b). This motion consists of periodic pulses. Figure A.4 (c) presents the

[1]The physical parameters employed reflect those of the Kloof mine winder - $V_e = 15m/s, R_d = 2.14m, d = 48mm, \beta = 0.2rad$, where V_e, R_d, d, β represent the nominal winding velocity, the drum radius, the rope diameter and the cross over arc respectively. Note that these plots reflect the displacement amplitudes for an upwind on the second layer ie. u is negative whilst the rope is traversing in the positive v direction. The displacement profile u is calculated continuously with respect to the cross-over arc β, via $u(\theta) = [(R_d\theta)^2 + (\frac{d\theta}{2\beta})^2 + (\frac{2v_n\theta}{\beta})^2]^{\frac{1}{2}} - R_d\theta \qquad 0 \leq \theta \leq \beta/2$, and a similar relationship for $\beta/2 \leq \theta \leq \beta$. The displacement profile v is calculated as a triangular pulse of magnitude $(1 - \sqrt{3}/2)d$. The displacement profile w is calculated as a ramp of magnitude $d/2$.

lateral out-of-plane displacement w, and reflects the total lateral displacement for one revolution. This displacement comprises of both the average traverse velocity (reflected by the dotted line) and the periodic displacement at the coil cross-over, as presented in Figure A.5.

The Fourier spectra of the periodic wave-forms presented in figure A.5 are presented in figure A.6. Figure A.7 presents the periodic wave forms and their reconstruction from the first and second harmonics of the Fourier spectrum. The periodic displacement functions are:

$$u(t) = \sum_{n=1}^{2} Re(U_n e^{jn\Omega t})$$

$$v(t) = \sum_{n=1}^{2} Re(V_n e^{jn\Omega t})$$

$$w(t) = \sum_{n=1}^{2} Re(W_n e^{jn\Omega t})$$

The harmonic amplitudes U_n, V_n, W_n are complex and contain both amplitude and phase information. For a 180^o Lebus liner, the excitation frequency Ω is related to the nominal winding velocity V_e and the drum diameter R_d by:

$$\Omega = 2V_e/R_d$$

It is evident from the spectra presented in figure A.6 that the most significant excitation occurs in the out-of-plane lateral direction (w), and is an order of magnitude larger than the first harmonic of the in-plane lateral excitation v. Although the longitudinal excitation is small, the axial stiffness is high and consequently significant periodic axial forces can be generated[2].

The displacement profiles presented in figures A.4,A.5 were constructed numerically. A Fourier transform of the displacement profiles provided the amplitude and phase information of each wave form. In this way, both the magnitude and phase relationships between the longitudinal and lateral excitations can be assessed for use in either the stability analysis, or the numerical simulation[3].

[2]Dimitriou and Whillier [1973] estimate the axial forces due to the longitudinal excitation to be of the order of 5KN.

[3]This definition was applied in the non-linear normal mode simulation. An alternative definition, as applied by Mankowski, was applied to the quasi-static model, and is defined in section A.4

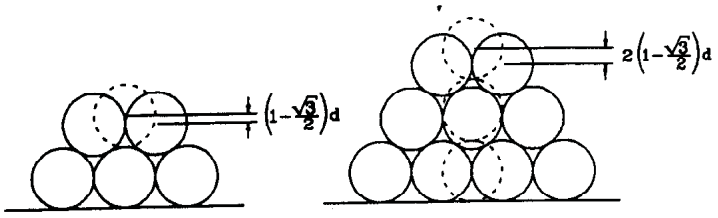

Figure A.2: Geometry of rope layers

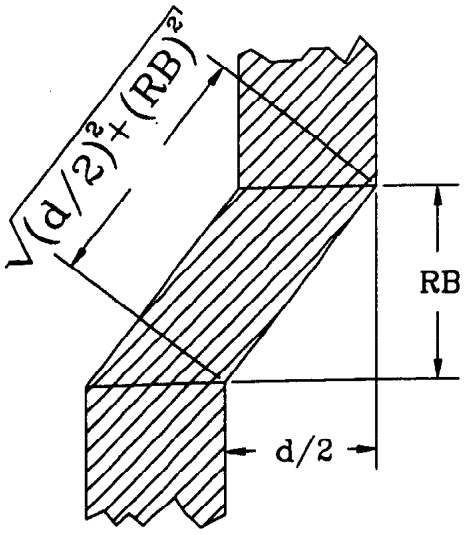

Figure A.3: Cross-over geometry

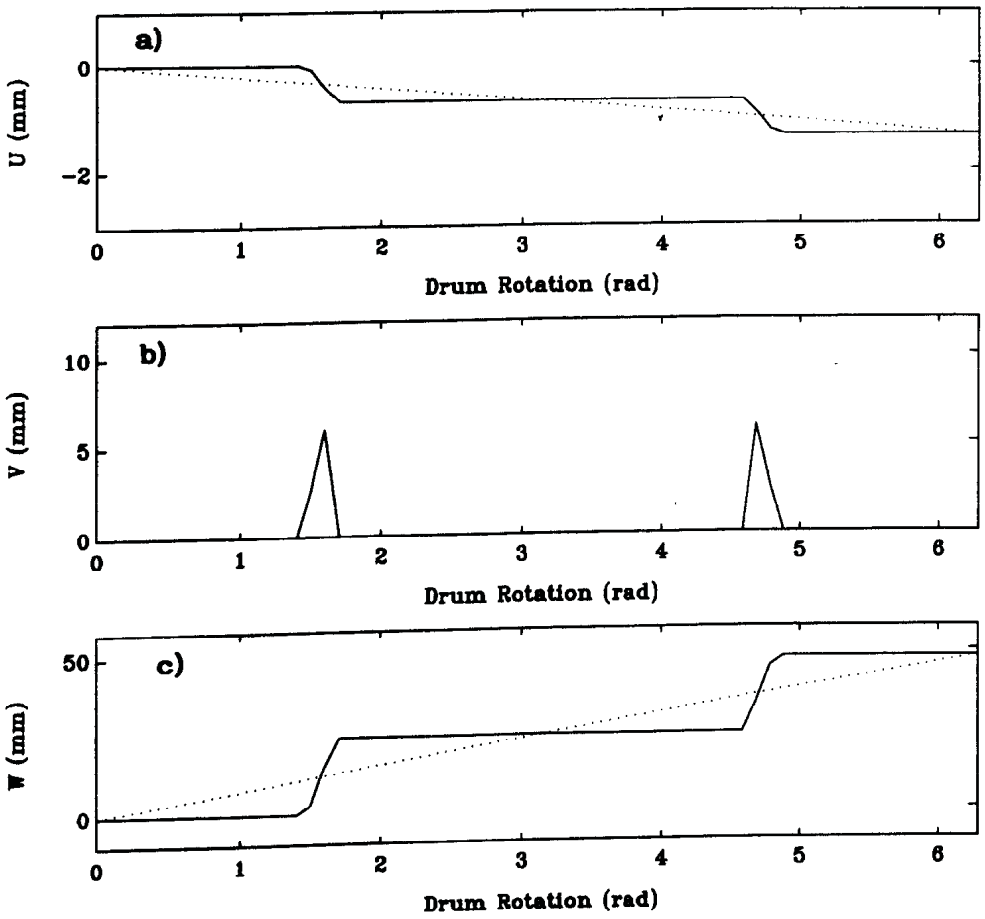

Figure A.4: Physical rope motion per drum revolution

(a) Longitudinal Motion u
(b) In-plane Lateral Motion v
(c) Out-of-plane Lateral Motion w

$V = 15m/s$, $\beta = 0.2rad.$, $d = 48mm$, $R_d = 2.14m.$

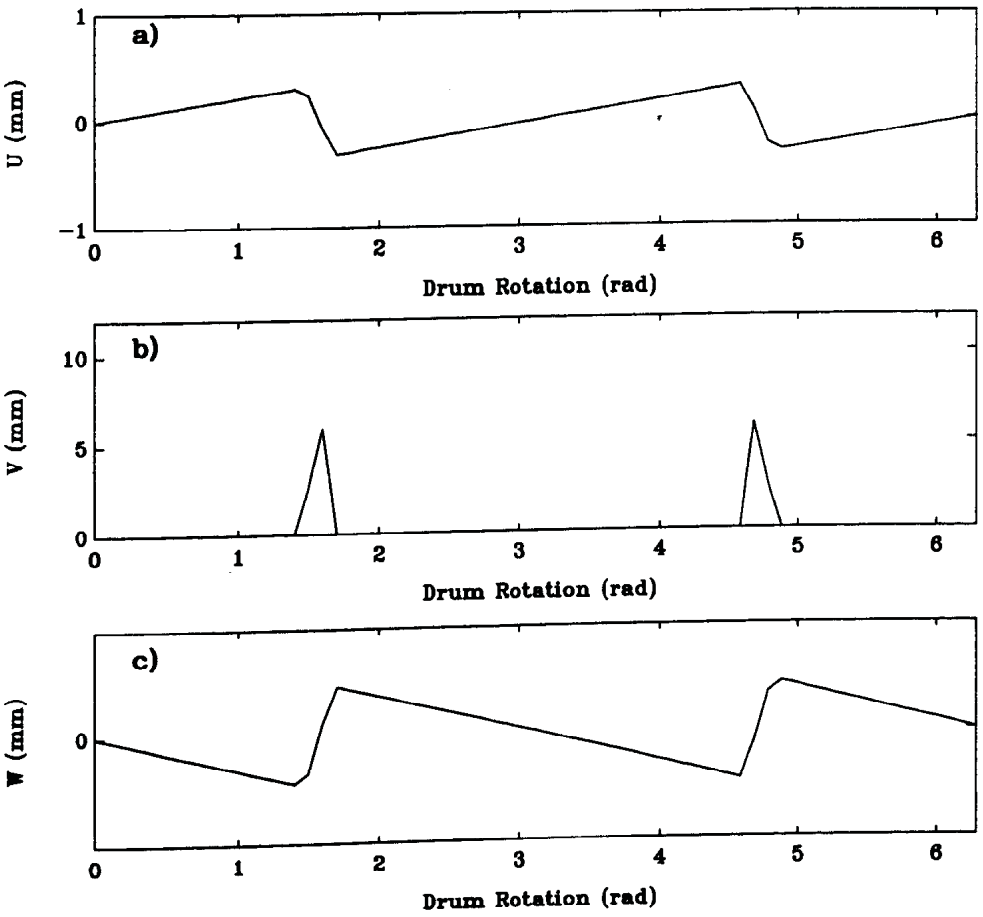

Figure A.5: Periodic motion per drum revolution

(a) Longitudinal Motion u
(b) In-plane Lateral Motion v
(c) Out-of-plane Lateral Motion w

$V = 15m/s$, $\beta = 0.2rad.$, $d = 48mm$, $R_d = 2.14m.$

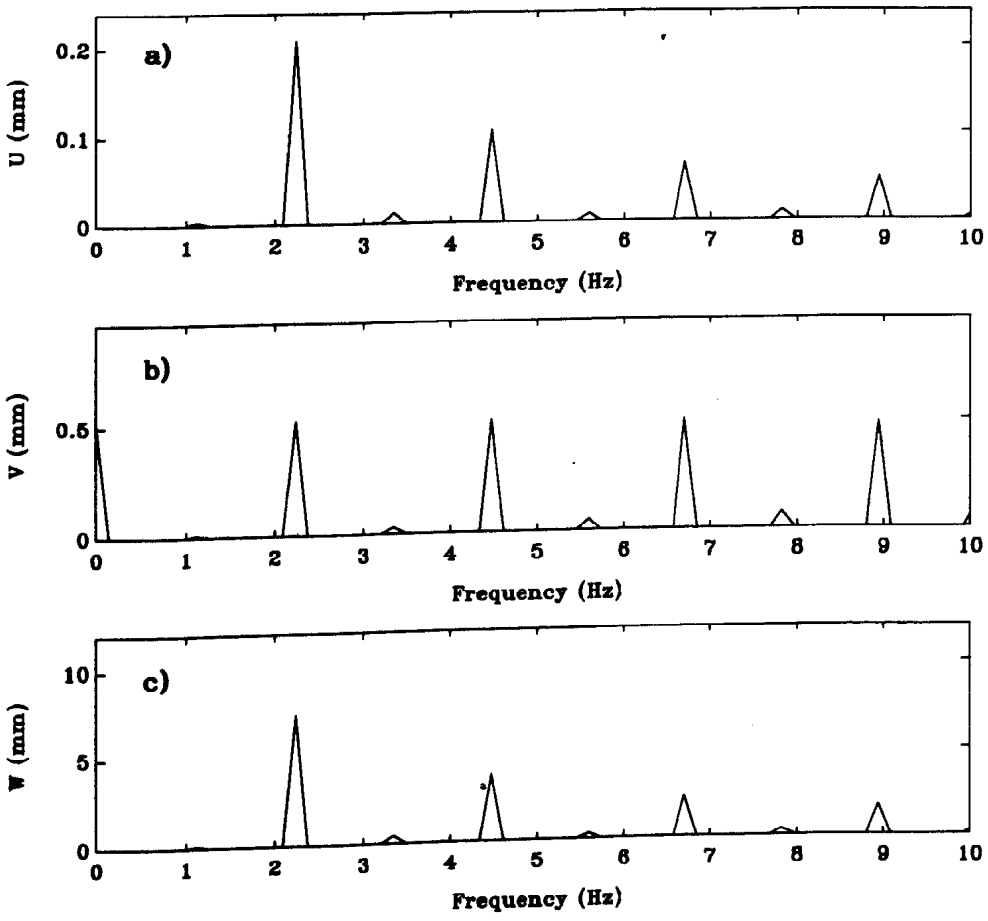

Figure A.6: Displacement spectra

(a) Longitudinal Spectrum u
(b) In-plane Lateral Spectrum v
(c) Out-of-plane Lateral Spectrum w

$V = 15m/s$, $\beta = 0.2rad.$, $d = 48mm$, $R_d = 2.14m.$

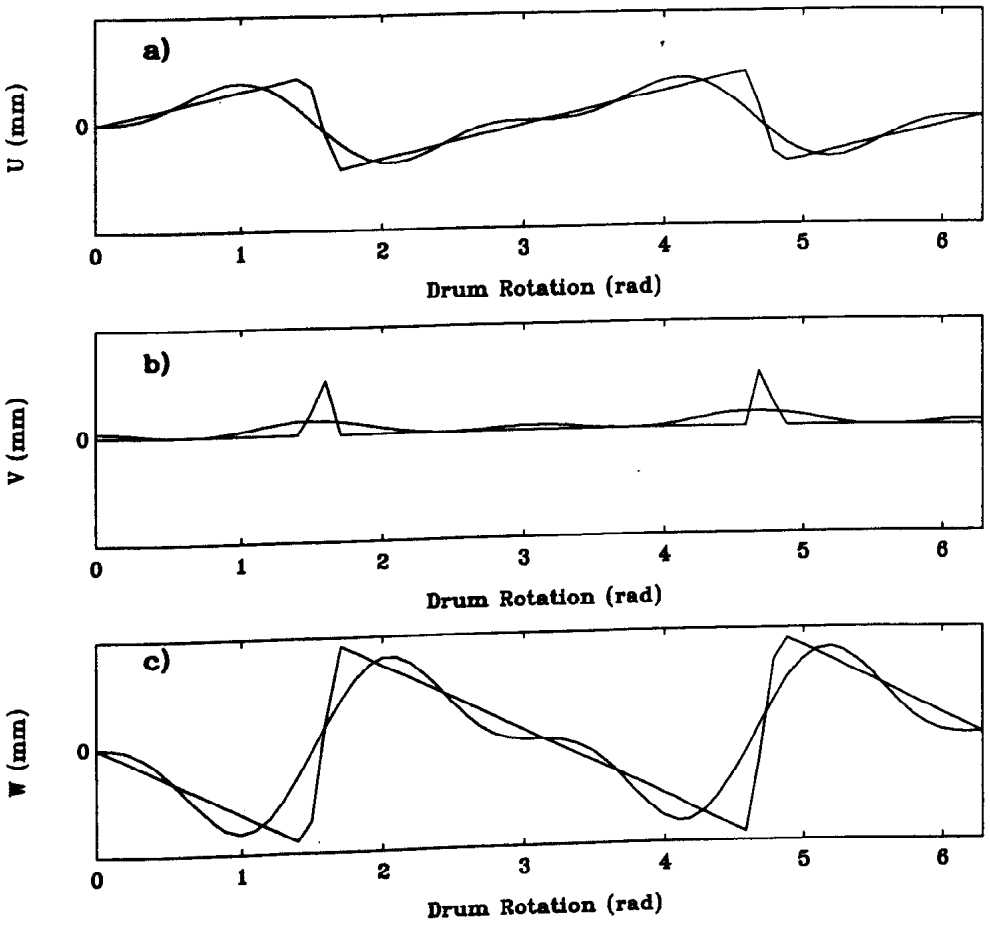

Figure A.7: Simulated Fourier vs. physical excitation - 2 Harmonics

(a) Longitudinal Motion u
(b) In-plane Lateral Motion v
(c) Out-of-plane Lateral Motion w

$V = 15m/s$, $\beta = 0.2rad.$, $d = 48mm$, $R_d = 2.14m.$

A.2 Acceleration/Deceleration Excitation

The longitudinal transient response of the system due to the initial acceleration or deceleration profile is commonly viewed as the most significant aspect of the dynamic response. Consequently many studies in the mining industry have focussed on longitudinal oscillations such as Vaughan[1903, 1917], Pollock and Alexander[1951], Perry and Smith[1932], Greenway[1989], whilst neglecting the coupled dynamics of the catenary. The inertial loading due to the acceleration and deceleration profile is significant and is modelled in modal space by applying a co-ordinate transformation to the system. Considering the inertial term in the longitudinal equation of motion $[1+\zeta\delta(l_c)+\eta\delta(l_v)]u_{tt}$, where $\zeta = I/\rho AR^2$ and $\eta = M/\rho A$, and applying a co-ordinate transformation:

$$u = \boldsymbol{u} + \overline{u}(t)$$

where $\boldsymbol{u}$ represents the dynamic motion at any point along the rope relative to an axial rigid body motion $\overline{u}(t)$. Since the rigid body motion is not a function of the spatial variable, the equivalent inertial load applied to the system is:

$$F(s,t) = -[1+\zeta\delta(l_c)+\eta\delta(l_v)]\ddot{\overline{u}}(t)$$

This load is evaluated in modal space as:

$$P_i(t) = -\frac{1}{m^u_{ii}}\int_0^{l_c+l_v}[1+\zeta\delta(l_c)+\eta\delta(l_v)]\ddot{\overline{u}}(t)\phi(s)ds$$

where $P_i(t)$ represents the equivalent modal force applied to the i^{th} mode; $\ddot{\overline{u}}(t)$ represents the acceleration or deceleration of the system; m_{ii}, ϕ_i represent the modal mass and mode shape of the i^{th} longitudinal mode respectively, as defined in Appendix C for the normal mode model.

A.3 Layer Change Excitation

At a layer change the effective radius of the drum increases/decreases by one rope diameter (d) over the cross-over arc, during the up or down wind respectively. Immediately after this, the rope reverses its direction of traverse. The reversal of the transverse motion causes the lateral out-of-plane excitation to change in phase by 180°. If the winder is treated as an ideal energy source, with a constant drum speed, then in order to accommodate the effective change in diameter at a layer change, the rope experiences a velocity change in a direction tangential and normal to the drum surface. The change in velocity results in a longitudinal and in plane lateral acceleration of the system, and consequently longitudinal and lateral in plane transient response. Since the system is non-linear, these pulses may pre-empt a jump to an alternative dynamic state. For this reason, this excitation source has been included in the analysis. A simple approach is developed below to approximate the acceleration pulse induced by a layer change.

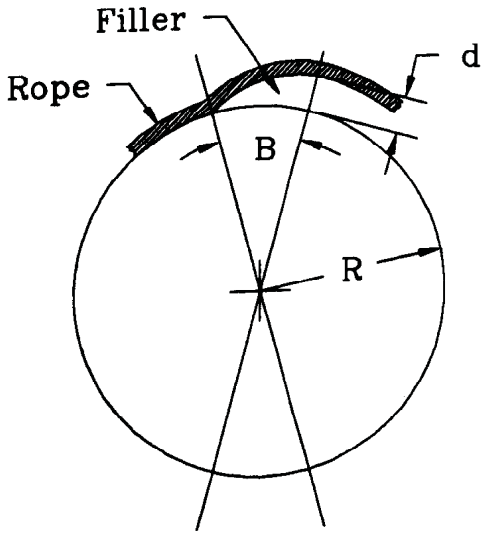

Figure A.8: Filler geometry

In figure A, the detail of a 180° Lebus liner is presented, whilst figure A.8 presents a section of the liner at the drum flange. A filler is positioned on the drum flange to achieve a layer change. In this figure, the layer change occurs over an arc length β. If it is assumed that the winder is an ideal energy source, then the angular velocity of the drum ω remains constant. During the layer change the rope changes its radial position by one rope diameter. If it is assumed that the radial profile is:

$$r(\theta) = dsin^2(\frac{\pi\theta}{2\beta})$$

For a constant angular velocity ω of the drum, $\theta = \omega t$:

$$r(t) = dsin^2(\frac{\pi\omega t}{2\beta})$$

The radial acceleration of the rope is given as:

$$\ddot{r}(t) = \frac{1}{2}d(\frac{\pi\omega}{\beta})^2 cos(\frac{\pi\omega t}{\beta})$$

The axial acceleration is determined from the change of the arc length s of the profile.

$$s(\beta) = \int_0^\beta [1 + \frac{1}{R_d^2}(\frac{dr}{d\theta})^2]^{\frac{1}{2}} R_d d\theta$$

Substituting for the profile $r(\theta)$ and simplifying:

$$s(\theta) = R_d\beta + \frac{1}{2R_d}(\frac{\pi d}{2\beta})^2 \int_0^\beta sin^2(\frac{\pi\theta}{\beta})d\theta$$

Converting to the time domain and carrying out the differentiation with respect to time:

$$\ddot{s}(t) = \frac{\omega}{2R_d}(\frac{\pi d}{2\beta})^2(\frac{\pi\omega}{\beta})sin(\frac{2\pi\omega t}{\beta})$$

In view of the previous section, the additional loading in the longitudinal modal co-ordinates, for the normal mode model, is given by:

$$P_i(t) = -\frac{1}{m_{ii}^v}\int_0^{l_c+l_v} \ddot{s}(t)[1+\zeta\delta(l_c+\eta\delta_{l_v}]\phi(s)ds$$

In the quasi-static model, the longitudinal excitation due to the layer change is applied through a displacement at the drum. Across the arc of the layer change, this displacement is given by:

$$u_l(\theta) = \frac{1}{2R_d}(\frac{\pi d}{2\beta})^2\int_0^{\beta} sin^2(\frac{\pi\theta}{\beta})d\theta$$

This displacement is held constant until the next layer change, where an additional displacement function is applied in a step-wise manner until the end of the wind.

A co-ordinate transformation is applied to account for the inertial loading in the in-plane lateral direction. Since the catenary is restrained in the lateral direction at the sheave end, the displacement varies from that at the drum, linearly to zero at the sheave. Thus the co-ordinate transformation applied is:

$$v = \overline{v} + (1-\frac{s}{l_1})r(t)$$

where $\overline{v}$ represents the dynamic motion of the cable with respect to the rigid body motion $r(t)$. Thus the distributed inertial loading is:

$$F_v(s,t) = -(1-\frac{s}{l_1})\ddot{r}(t)$$

This equivalent modal load applied to the i^{th} mode can be evaluated in the usual manner as:

$$Q_i(t) = -\frac{1}{m_{ii}^w}\int_0^{l_c} \ddot{r}(t)(1-\frac{s}{l_c})\Phi(s)ds$$

where m_{ii}, Φ_i represent the modal mass and mode shape of the i^{th} lateral mode respectively.

These loads are calculated at the appropriate time during the wind. It is interesting to note that since the layer change occurs over a short time interval, the radial acceleration is significant and is of the order of 30g, whilst that of the axial acceleration is of the order of 2g. Figure A.9 presents a plot of the physical rope displacement in the region of the layer change, and the associated axial and normal acceleration of the rope, as a function of drum rotation. It is pertinent to note that radial acceleration is inversely proportional to the square of the arc length, whilst the axial acceleration is inversely proportional to the cube of the arc length (β); thus the layer change transient can be significantly reduced by increasing the riser and cross-over arc[4].

[4]A long filler is undesirable since it leads to additional wear of the rope strands. Experience regarding the cross-over arc length is that the stability of the coiling pattern is adversely affected with an increase in the cross-over arc. Currently the maximum cross-over arc is of the order of 30°.

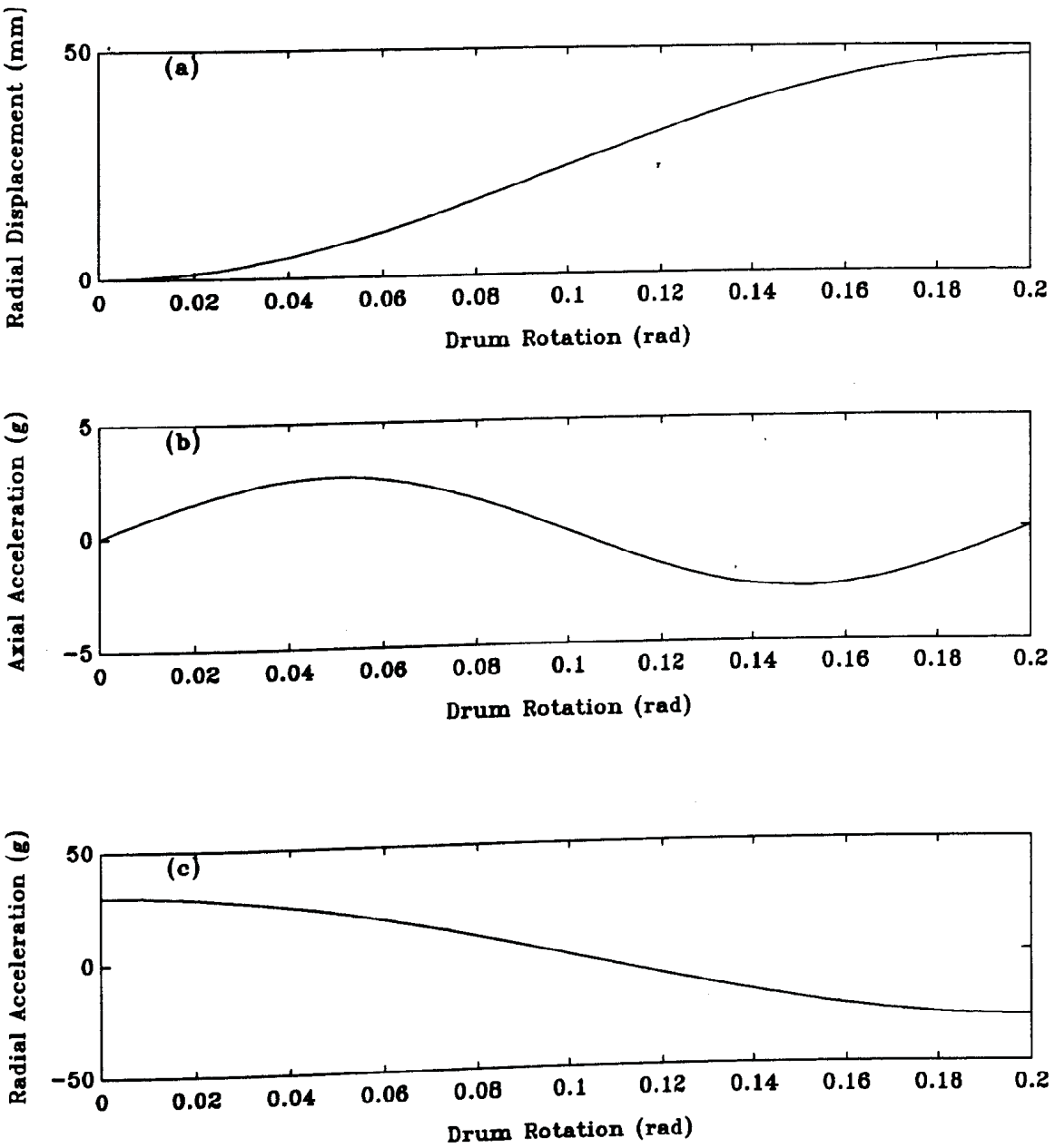

Figure A.9: Layer change transient excitation

(a) Radial Displacement (mm)
(b) Radial Acceleration $\ddot{r}(t)$ (g)
(c) Axial Acceleration $\ddot{s}(t)$ (g)

$V = 15m/s$, $\beta = 0.2rad.$, $d = 48mm$, $R_d = 2.14m.$

A.4 Excitation Definition for the Quasi-Static Model

In developing the quasi-static model with the Simulink software, it was possible to define the geometry of the coil cross over region by means of a look-up table. This is advantageous since the impulsive nature of the excitation is retained for little additional computational effort. Mankowski[1982] defined the coil cross over excitation by means of versine functions in terms of the period of the Lebus frequency τ, the duration of the Lebus cross-over τ_β, and the delay time between two successive layer cross overs τ_d. The forcing function displacements are illustrated in figure (A.10). These functions are defined by:

$$\tau = \pi R_d / V_e$$
$$\tau_\beta = \tau\beta/\pi$$
$$\tau_d = \tau - \tau_\beta$$
$$\omega = \pi/\tau_\beta$$

$$u(0,t) = \tfrac{1}{2}\overline{U}[1 - cos(\omega t)] \quad 0 < t \leq \tau_\beta$$
$$v(0,t) = \tfrac{1}{2}\overline{V}[1 - cos(2\omega t)] \quad 0 < t \leq \tau_\beta$$
$$w(0,t) = \tfrac{1}{2}\overline{W}[1 - cos(\omega t)] \quad 0 < t \leq \tau_\beta$$

$$u(0,t) = \overline{U}[t - \tau_\beta]/\tau_d \quad \tau_\beta < t \leq \tau$$
$$v(0,t) = 0 \quad \tau_\beta < t \leq \tau$$
$$w(0,t) = d/2 \quad \tau_\beta < t \leq \tau$$

where $u(0,t)$, $v(0,t)$, $w(0,t)$ refers to the periodic forced displacement at the drum in the longitudinal, in-plane lateral, and out-of-plane lateral directions respectively; d refers to the rope diameter, β refers to the arc of the layer cross over region, V_e the surface speed of the drum, and R_d refers to the winder drum radius.

$$\overline{U} \approx (0.125 + 0.018(n-1)^2)d^2/R_d\beta$$
$$\overline{V} = (n-1)(1 - \sqrt{3}/2)d = 0.134(n-1)d$$
$$\overline{W} = d/2$$

where $\overline{U}, \overline{V}, \overline{W}$ are determined by considering the geometry of the layer cross-over region, and n represents the layer number. The lateral excitation is applied to the catenary by a co-ordinate transformation, which results in an equivalent inertial load being applied in the transformed reference frame. The versine function is easily differentiated in the cross-over region allowing the forcing function to be defined as a function of shaft depth for the in and out-of-plane lateral modes, and defined in a look-up table.

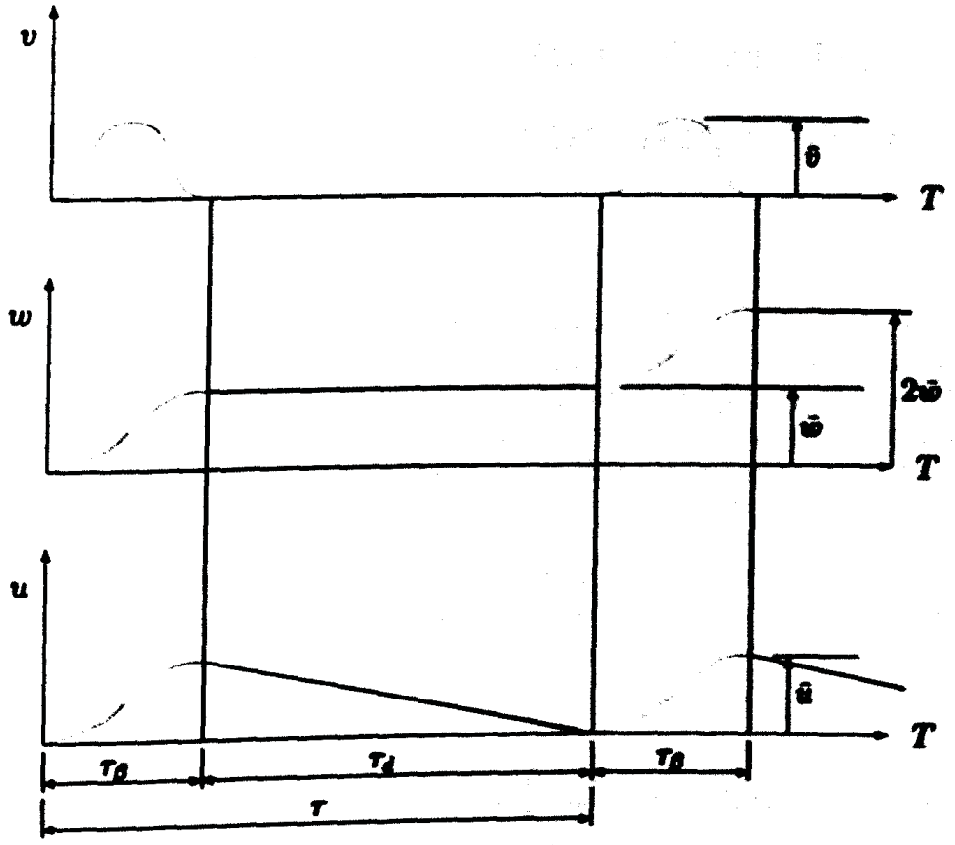

Figure A.10: Lebus coil-cross over excitation - Versine functions

Appendix B

Parametric Response due to Longitudinal Excitation Only

This appendix documents work carried out in the early stages of the study, where the lateral stability of the catenary was examined in the absence of cable curvature and axial transport velocity, due to stationary longitudinal excitation at the winder drum. The equations of motion developed in chapter 3, including relative proportional viscous damping and excluding cable curvature and axial transport velocity are:

$$\begin{aligned}(1+\zeta\delta(s-l_1)+\eta\delta(s-l_2))u_{tt} &= c^2u_{ss}+\mu u_{t,ss}\\ &+c^2(v_sv_{ss}+w_sw_{ss})[H(s)-H(s-l_1)]\end{aligned} \tag{B.1}$$

$$v_{tt} = \bar{c}^2v_{ss}+\mu_l v_{t,ss}+c^2\left[(u_sv_s)_s+\tfrac{3}{2}(v_s)^2v_{ss}+\tfrac{1}{2}(w_s^2v_s)_s\right] \tag{B.2}$$

$$w_{tt} = \bar{c}^2w_{ss}+\mu_l w_{t,ss}+c^2\left[(u_sw_s)_s+\tfrac{3}{2}(w_s)^2w_{ss}+\tfrac{1}{2}(v_s^2w_s)_s\right] \tag{B.3}$$

Where s refers to the axial co-ordinate measured along the rope from the drum to the suspended mass. l_1, l_2 refer to the length of the catenary and total length of the rope respectively. c^2, and $\bar{c}^2$ represent the longitudinal and lateral wave speeds. $\zeta = \frac{I}{\rho AR^2}, \eta = \frac{M}{\rho A}$, and I, R, M, E, A refer to the sheave inertia, sheave radius, conveyance mass, modulus of elasticity, and effective steel area of the rope respectively. μ, μ_l represent the longitudinal and lateral

damping mechanism respectively. Lateral damping is low, of the order of 0.02% of critical, and will consequently be discarded at this stage of the analysis. Longitudinal damping is more appreciable, and is of the order of 1.5% for the first mode, and is therefore retained. Damping is discussed in more detail in chapter 5[1].

In the absence of lateral excitation, the lateral motion may be assumed to be trivial, and hence the response of the rope is purely longitudinal. The purpose of the analysis was to examine where such a solution would be stable. In the absence of lateral motion, the longitudinal equation of motion reduces to:

$$(1 + \zeta\delta(s - l_1) + \eta\delta(s - l_2))u_{tt} = c^2 u_{ss} + \mu u_{t,ss} \tag{B.4}$$

This is a linear equation, and the steady state longitudinal response due to harmonic excitation at the winder drum, $u(0,t) = Re(\sum_{n=1}^{i} U_n e^{jn\Omega t})$, can be formulated in closed form[2]. The axial system response in the catenary section of the rope to such an excitation is presented in appendix C as:

$$u(s_1,t) = Re[\sum_{n=1}^{i}[A_n cos\lambda_n s + B_n sin\lambda_n s]e^{jn\Omega t}]$$

where $\lambda_n = \frac{n\Omega}{c}$, and A_n, B_n are defined in Appendix C.

On substituting the solution for the longitudinal response into equations (B.2),(B.3), the linearised form of the lateral variational equations of motion contain identical terms, and thus only one of the two need be considered. Instability of the trivial solution predicts departure from longitudinal motion to non-planar motion. The severity of this motion will depend on the nonlinear nature of the system, and whether internal resonance occurs, which would further promote the coupling between the lateral and longitudinal motion. The linearised variational equation governing the lateral stability of the catenary is:

$$v_{tt} = \bar{c}^2 v_{ss} + c^2 [u_s v_s]_s \tag{B.5}$$

[1]This model accounts for relative proportional viscous damping, and consequently the modal damping factor increases in proportion to the natural frequency, and the higher modes become successively more damped. On site drop test measurements are presented in appendix G, and indicate that a general proportional damping mechanism may be more appropriate.

[2]Ω represents the coil cross-over frequency.

This equation is converted to an ordinary differential equation with periodic coefficients by applying an eigenfunction expansion for $v(s,t)$ as:

$$v(s,t) = \sum_{i=1}^{n} \phi_i(s) q_i(t) \tag{B.6}$$

where the eigenfunction $\phi_i(s)$ which satisfies the boundary conditions is:

$$\phi_i(s) = sin(\frac{i\pi}{l_1}s)$$

Substitution of equation (B.6) into equation (B.5), and orthogonalising with respect to $\phi_i(s)$ results in a set of coupled ordinary differential equations with periodic coefficients:

$$\left\{ \ddot{q} \right\} + \left[\begin{array}{cc} \backslash & \\ & \omega_i^2 \\ & & \backslash \end{array} \right] + \sum_{n=1}^{i} \left[\left[\begin{array}{cc} & \\ & D_{ij} \\ & & \end{array} \right]_n cos(n\Omega t) \right] \left\{ q_i \right\} = \left\{ \begin{array}{c} 0 \\ \end{array} \right\} \tag{B.7}$$

The parametric coupling matrix $[D_{ij}]_n cosn\Omega t$ is identical to that derived in Appendix F for $[W_{ww}(n\Omega t)]^1$, where the axial harmonics of the excitation $U_n e^{jn\Omega t}$ are in phase or 180° out of phase.

$$[D_{ij}]_n cosn\Omega t = Re([W_{ww}(n\omega t)])$$

B.1 Stability Analysis

The variational equations of motion governing the lateral stability of the system are linear equations with time varying coefficients. At this stage of the study, the lateral stability of the system due to longitudinal excitation was considered as a potential indicator for large amplitude catenary motion. Dimitriou and Whillier[1973], Mankowski[1982] and Backeberg[1984] were aware of the potential influence of parametric excitation and response, however no formal mathematical development was performed to examine this phenomenon. Intuitive criteria centred around the observation that regions of main parametric resonance[3] may exist where a lateral mode tunes to half the frequency of the Lebus coil cross-over frequency. This is often termed subharmonic resonance, as identified by Dimitriou and Whillier[1973], where lateral response occurs at a subharmonic of the axial excitation frequency. Dimitriou and Whillier[1973] discussed subharmonic resonance with regard to the experiment of Melde (1859), and the analysis of Lubkin and Stoker[1943]. In this discussion, It was proposed that subharmonic resonance would be amplified if a longitudinal mode was simultaneously resonant. Dimitriou and Whillier[1973] did not identify this condition with internal resonance, where the longitudinal mode tunes to twice the lateral mode, and consequently the nonlinear coupling which subsequently arises, where autoparametric resonance conditions develop. It was recognised that regions of combination resonance in mechanical systems had been reported in the literature, but as no formal analysis was performed proving their existence in the context of the mine hoist system, they were not considered.

The complexity of the mine rope problem is compounded by the fact that in reality the rope is moving with an axial transport velocity, and consequently the natural frequencies of the system are continuously changing. This effect is of considerable importance in the mine hoist system, since the travelling system may pass through a region of instability sufficiently rapidly to contain the growth of the lateral amplitude to an acceptable value. Thus in reality the importance of the region of instability is likely to be a function of both the transport velocity and the amplitude of the parametric excitation. This conforms to the case of a parametrically excited system with non stationary parameters, as discussed by by Nayfeh and Asfar[1988], Neal and Nayfeh[1990], and considered extensively by Mitropolskii[1965].

[3]Main parametric resonance occurs when $\Omega_p = 2\omega_i$.

B.2 Parametric Resonance of MDOF Systems

Hsu[1963] considered the primary regions of instability of a a multi-degree of freedom system subjected to periodic parametric excitation, where the periodic excitation was represented as a Fourier expansion containing an infinite series of harmonic functions. In his method, a perturbation approach was applied to analyse the size of the regions of parametric instability, when the parametric coupling terms are small. Nayfeh[1973a, 1992] reconsidered this and other problems related to parametrically excited linear and non-linear systems, by applying the method of multiple scales . More recently Szemplinska-Stupnika[1978] and Takahashi[1981a] have extended the method of the generalised harmonic balance as proposed by Bolotin[1964], to include combination resonance regions. Unlike perturbation techniques, the harmonic balance methods are not limited to the concept of a small parameter. The use of ultraspherical polynomial approximation techniques, employing Floquet stability theory have also been proposed (Sinha et al.[1979], Srinivasan and Sankar[1974]. The latter methods are computationally intensive for any sizeable system. Hsu's[1963] method was initially applied to study the system. In retrospect, Nayfeh's[1973b] method of multiple scales is more convenient, as it results in a uniformly valid expansion, and does not require the averaging techniques applied by Hsu[1963].

Hsu's[1963] results may be applied directly to a system of equations of the form:

$$\{\ddot{x}\} + \left(\epsilon \sum_{s=1}^{S} [D^s] cos s\omega t + [\omega_i^2]\right) \{x\} = \{0\}$$

where $[D]^s$ represents the parametric coupling matrix of the s^{th} harmonic, which may be a non-symmetric full matrix, and $[\omega_i^2]$ is a diagonal matrix with its terms equal to the square of the linear natural frequencies of the system, which are assumed to be distinct, and s refers to the s^{th} harmonic of the excitation frequency ω.

B.2.1 Hsu's Perturbation Solution

In analysing the system, Hsu[1963] represented the equations of motion in first order form as:

$$\begin{aligned} \frac{dx_i}{dt} &= w_i \\ \frac{dw_i}{dt} + \omega_i^2 x_i &= f_i(x_i, \omega_i, t) \end{aligned} \tag{B.8}$$

where the solution $x_i(t)$ contains a component representing the free response of the linear solution, and a power series expansion in the perturbation term ϵ:

$$x_i(t) = A_i(t)cos\omega_i t + B_i(t)sin\omega_i t + \sum_{q=1}^{n} \epsilon^q x_i^{(q)} \tag{B.9}$$

$$w_i = \frac{dx_i}{dt} = \omega_i(-A_i(t)sin\omega_i t + B_i(t)cos\omega_i t) + \sum_{q=1}^{n} \epsilon^q \frac{dx_i^{(q)}}{dt} \tag{B.10}$$

The first two terms on the right hand side of these equations are termed the variational part of the solution, whilst the remaining term is the perturbation part of the solution. In essence the variational component of the solution represents the response of the system to an initial disturbance or a variation of the trivial solution. If this component of the solution is stable, then the disturbance remains bounded, and the response to the disturbance is essentially dictated by the free response of the system. However in a region of instability, the variational component of the solution grows without bound, indicating that the system is unstable if subjected to an arbitrarily small disturbance.

In equation (B.10) above, A_i, B_i are assumed to vary slowly with time, and consequently are assumed time independent, when differentiating with respect to time. However, since A_i, B_i may be functions of time, the condition of slowly varying parameters is satisfied only when:

$$\frac{dA_i}{dt}cos\omega_i t + \frac{dB_i}{dt}sin\omega_i t = 0$$

Substitution of the assumed solution (B.9), into the equation motion (B.8) results in:

$$\begin{aligned}\omega_i(-A_i^{'}sin\omega_i t - \omega_i A_i cos\omega_i t &+ B_i^{'}cos\omega_i t - \omega_i B_i sin\omega_i t) + \\ \omega_i^2(A_i cos\omega_i t + B_i sin\omega_i t) &+ \omega_i^2 \sum \epsilon^q x_i^q + \sum \epsilon^q \frac{d^2 x_i^q}{dt^2} \\ &= -\epsilon \left\{ \sum_{s=1}^{S} \sum_{j=1}^{n} d_{ij}^s cossc\omega t x_j \right\} \end{aligned} \tag{B.11}$$

Considering only the first order powers[4] of ϵ and equating terms, the following system of equations are obtained; the solution of which determines the coefficients A_i, B_i:

$$\frac{dA_i}{dt} cos\omega_i t + \frac{dB_i}{dt} sin\omega_i t = 0 \tag{B.12}$$

$$\begin{aligned} -\omega_i \frac{dA_i}{dt} sin\omega_i t + \omega_i \frac{dB_i}{dt} cos\omega_i t &+ \epsilon(\frac{d^2 x_i^1}{dt^2} + \omega_i^2 x_i^1) = \\ &- \frac{\epsilon}{2} \sum_{s=1}^{S} \sum_{j=1}^{n} \{ d_{ij}^s A_j (cos(\omega_j + s\omega)t \\ &+ cos(\omega_j - s\omega)t) + d_{ij}^s B_j (sin(\omega_j + s\omega)t \\ &+ sin(\omega_j - s\omega)t)\} \end{aligned} \tag{B.13}$$

Hsu[1963] then proceeded by considering the variational and perturbation part of the solution separately. Those terms which result in small divisors are retained in the variational part of the solution, whilst the remaining terms are carried to the perturbation component of the solution. If one assumes that the system is tuned such that ω_i are distinct and $\omega_j \pm s\omega$ are not close to $\pm\omega_i$, then all the terms on the right hand side of equation (B.13) are retained in the perturbation part of the solution, which is bounded. The equations describing the variational part of the solution are:

[4]Expansions developed to higher order would define the second and subsequent regions of instability. These are known to be smaller and more difficult to enter than the primary region, and consequently only the primary parametric region is considered by Hsu[1963].

$$\frac{dA_i}{dt}cos\omega_i t + \frac{dB_i}{dt}sin\omega_i t = 0$$
$$-\frac{dA_i}{dt}sin\omega_i t + \frac{dB_i}{dt}cos\omega_i t = 0 \qquad \text{(B.14)}$$

Solving for A_i, B_i leads to constant coefficients, and thus the solution is bounded and stable.

However in cases where $\omega_j \pm s\omega$ is close to $\pm\omega_i$, the stability of the system must be examined as small divisor terms occur in the perturbation part of the solution $x^{(q)}$, and are consequently carried to the variational part of the solution. The variational equations can be transformed into a set of autonomous equations by applying the Kryoloff-Bogoliuboff-Van der Pohl averaging technique, where it is assumed that A_i, B_i are slowly varying functions of time relative to the averaging period, and are therefore treated as constants. The stability of these autonomous equations, and consequently the stability of the variational solution, can then be determined by examining the characteristic roots of the autonomous equations.

Proceeding in this manner, Hsu[1963] determined that for an undamped system, the motion would be unstable and grow without bound if the following conditions were satisfied.

$\omega = \frac{2\omega_i}{s}$	Main parametric resonance
$\omega = \frac{1}{s}(\omega_i \pm \omega_j)$	Combination parametric resonance

Further analysis provides the regions of instability as a function of the perturbation coefficient ϵ. These regions are given by:

Main parametric resonance

$$\frac{2\omega_i}{s} - \frac{\epsilon|d_{ii}|^{(s)}}{2s\omega_i} < \omega < \frac{2\omega_i}{s} + \frac{\epsilon|d_{ii}|^{(s)}}{2s\omega_i}$$

Combination sum type parametric resonance:

$$\frac{\omega_i + \omega_j}{s} - \frac{\epsilon}{2s}\left(\frac{d_{ij}^{(s)}d_{ji}^{(s)}}{\omega_i\omega_j}\right)^{\frac{1}{2}} < \omega < \frac{\omega_i + \omega_j}{s} + \frac{\epsilon}{2s}\left(\frac{d_{ij}^{(s)}d_{ji}^{(s)}}{\omega_i\omega_j}\right)^{\frac{1}{2}}$$

Combination difference type parametric resonance

$$\frac{\omega_i - \omega_j}{s} - \frac{\epsilon}{2s}\left(\frac{-d_{ij}^{(s)} d_{ji}^{(s)}}{\omega_i \omega_j}\right)^{\frac{1}{2}} < \omega < \frac{\omega_i - \omega_j}{s} + \frac{\epsilon}{2s}\left(\frac{-d_{ij}^{(s)} d_{ji}^{(s)}}{\omega_i \omega_j}\right)^{\frac{1}{2}}$$

These regions are termed main and combination sum and difference type resonances respectively. These results confirm that in a coupled system, the diagonal terms of the parametric coupling matrix $d_{ii}^{(s)}$ govern the size of the main parametric resonance region, whilst the off diagonal terms $d_{ij}^{(s)}$ govern the size of the combination parametric resonance region. Difference type resonances can only occur if $d_{ij}^{(s)} d_{ji}^{(s)} < 0$ and conversely sum type can only occur if $d_{ij}^{(s)} d_{ji}^{(s)} > 0$. Thus only sum type combination resonances will occur if the coupling matrix is symmetric, whilst both may occur if the matrix is asymmetric.